



**CHALMERS**  
UNIVERSITY OF TECHNOLOGY

---

# **Condensation induced water hammer**

Master's thesis in Applied Mechanics

**RAJUKIRAN ANTHAM**

---

Department of Applied Mechanics  
CHALMERS UNIVERSITY OF TECHNOLOGY  
Gothenburg, Sweden 2016



MASTER'S THESIS 2016:79

# Condensation induced water hammer

RAJUKIRAN ANTHAM



**CHALMERS**  
UNIVERSITY OF TECHNOLOGY

Department of Applied Mechanics  
*Division of Fluid Dynamics*  
CHALMERS UNIVERSITY OF TECHNOLOGY  
Gothenburg, Sweden 2016

Condensation induced water hammer  
RAJUKIRAN ANTHAM

© RAJUKIRAN ANTHAM, 2016.

Supervisor:

Daniel Edebro, Vattenfall AB, Daniel.Edebro@vattenfall.com  
Pascal Veber, Onsala Ingenjörbyrå AB, pascal@onsala-ing.se

Examiner:

Srdjan Sasic, Department of Applied Mechanics, srdjan@chalmers.se

Master's Thesis 2016:79  
Department of Applied Mechanics  
Division of Fluid Dynamics  
Chalmers University of Technology  
SE-412 96 Gothenburg  
Telephone +46 31 772 1000

Printed by [Chalmers Reproservice]  
Gothenburg, Sweden 2016

Condensation induced water hammer  
RAJUKIRAN ANTHAM  
Department of Applied Mechanics  
Division of Fluid Dynamics  
Chalmers University of Technology

## Abstract

Condensation is a commonly occurring phenomenon in many industries. Rapid condensation in horizontal channels may sometimes result in Condensation induced water hammers which are potentially violent and may result in serious damage. These transients are triggered by Direct contact condensation. The present work focuses on modelling of Direct contact condensation in a horizontal channel. Simulations are carried out using Ansys Fluent and the results are compared against experimental results from LAOKOON facility. Ansys Volume of fluid approach and condensation models based on surface renewal theory are used in the simulations. Different meshes and performance of the condensation models are investigated in the present work.

The simulation results achieved are mesh independent and corresponded well with the experiment results from LAOKOON facility. However, the thermal layer obtained in the simulations is thinner than the experiment. The reason for this might be because of using turbulence damping to obtain a smooth water surface.

Keywords: CIWH, DCC, Heat transfer coefficient, VOF, Surface renewal time, Turbulence damping.



## **Preface**

This master thesis is performed during the spring of 2016 and represents the final step in obtaining a Master's Degree in Applied Mechanics at Chalmers University of Technology. The master's thesis work has been carried out for Vattenfall AB in collaboration with Onsala Ingenjörbyrå AB.

## **Acknowledgements**

I would like to express my gratitude to Vattenfall AB for giving me the opportunity to perform this master thesis. I would like to acknowledge Onsala Ingenjörbyrå AB for providing me with the support and the computational resources. Many thanks to my supervisors Daniel Edebro at Vattenfall AB and Pascal Veber at Onsala for sharing their valuable knowledge and experience with me. I am grateful to all the employees at Onsala for being very welcoming and supportive, making me feel as a part of the group from week one. A special thanks to Parisa Razmkhah for all the support and inputs. At Chalmers, I would like to thank my examiner Professor Srdjan Sasic for being helpful and answering all my questions.

Finally, I would like to thank all my friends and family who have helped me in completion of this thesis.

Rajukiran Antham, Gothenburg, August 2016.



# List of Symbols

$\alpha$	Volume fraction
$\alpha_{tl}$	Thermal diffusivity
$\Delta t$	time step
$\dot{m}$	mass transfer
$\epsilon$	Dissipation
$\lambda$	Thermal conductivity
$\rho$	Density
$T$	cell averaged temperature
$T$	temperature
$t$	time
$V$	volume
$\mu$	Dynamic viscosity
$\nu$	Kinematic viscosity
$a_i$	Interfacial area density
$C_p$	Specific heat capacity
$g$	Gravitational acceleration
$h$	Enthalpy
$h_{lv}$	Latent heat
$k$	Turbulent kinetic energy
$L_t$	Turbulent eddy length scale
$Pr$	Prandtl number
$q$	heat flux
$t_{rp}$	Surface renewal time
$U$	Velocity
$V_t$	Turbulent eddy velocity scale

## List of Acronyms

<i>CFD</i>	Computational Fluid Dynamics
<i>CIWH</i>	Condensation Induced Water Hammer
<i>DCC</i>	Direct Contact Condensation
<i>ECCS</i>	Emergency Core Cooling System
<i>HTC</i>	Heat Transfer Coefficient
<i>IAD</i>	Interfacial Area Density
<i>LOCA</i>	Loss of Coolant Accident
<i>LSM</i>	Level Set Method

---

<i>SRT</i>	Surface Renewal Time
<i>SST</i>	Shear Stress Transport
<i>UDF</i>	User Defined Function
<i>VOF</i>	Volume of Fluid

## Sub scripts

<i>l</i>	liquid
<i>v</i>	vapor
<i>i</i>	interface
<i>t</i>	turbulent
<i>q</i>	phase index
<i>Sat</i>	saturation
<i>eff</i>	effective

# Contents

<b>List of Symbols</b>	<b>ix</b>
<b>List of Figures</b>	<b>xiii</b>
<b>List of Tables</b>	<b>xv</b>
<b>1 Introduction</b>	<b>1</b>
1.1 Background . . . . .	1
1.2 Objective . . . . .	2
1.3 Literature Survey . . . . .	2
<b>2 Theory</b>	<b>5</b>
2.1 Two-Phase flows . . . . .	5
2.2 Direct contact condensation . . . . .	7
2.3 Numerical Simulation of Two-Phase flow . . . . .	7
2.3.1 Two-Fluid Model . . . . .	7
2.3.2 Volume of Fluid Model . . . . .	9
2.4 Surface Renewal Theory . . . . .	10
2.4.1 Hughes and Duffey model . . . . .	11
2.4.2 Shen et al. model . . . . .	11
2.5 Description of LAOKOON experimental facility . . . . .	12
2.6 Implementation . . . . .	14
2.6.1 Temporal relaxation . . . . .	15
2.6.2 Turbulence Damping . . . . .	15
2.6.3 Calculation of Interfacial area density . . . . .	16
<b>3 Geometry and Mesh</b>	<b>17</b>
3.1 Domain Geometry . . . . .	17
3.2 Grid Generation . . . . .	17
3.3 Case setup . . . . .	18
<b>4 Results and discussion</b>	<b>21</b>
<b>5 Conclusion</b>	<b>27</b>
5.1 Future work . . . . .	27
<b>Bibliography</b>	<b>29</b>

<b>A Appendix 1</b>	<b>I</b>
A.1 User Defined Functions used . . . . .	I
A.2 Smearing Function . . . . .	IV

# List of Figures

1.1	Schematic representation of CIWH phenomenon [1] . . . . .	1
2.1	Two-phase flow patterns in horizontal flow [29] . . . . .	6
2.2	Volume fraction and properties in each cell [21] . . . . .	9
2.3	LAOKOON experimental set up [26] . . . . .	12
2.4	Flow wise cross section of LAOKOON experimental set-up [27] . . . .	13
3.1	Flow wise cross section of LAOKOON experimental set-up [26] . . . .	17
3.2	Mesh generated for LAOKOON facility . . . . .	18
4.1	Liquid volume fraction comparison at various locations across the channel. . . . .	21
4.2	Liquid volume fraction in the channel . . . . .	22
4.3	Comparison of the temperature profiles against LAOKOON experi- mental data. . . . .	23
4.4	Closer view of temperature profile in case-3. . . . .	23
4.5	Comparison between the HTC calculated at probe location with both condensation models . . . . .	24
4.6	Convergence plot for case-1 . . . . .	25



# List of Tables

2.1	Parameters of LAOKOON experimental set-up [27] . . . . .	13
2.2	Temperature data near thermocouple line [27] . . . . .	14
3.1	Material properties used in LAOKOON experiment [26]. . . . .	18
3.2	Cases simulated in this work . . . . .	19



# 1

## Introduction

Safety is given utmost priority in nuclear industry. Even though the safety systems are well regulated, certain thermo-hydraulic transients like the condensation induced water hammer (CIWH) may occur during Loss of Coolant Accident (LOCA) event. CIWHs are highly stochastic, violent and may result in potential damage of mechanical components. These transients are triggered by Direct contact condensation (DCC) of steam on subcooled liquid. A reliable prediction of the DCC is necessary to study the CIWH. The realistic modelling of interfacial heat and mass transfer during DCC depends on accurate modelling of the heat transfer coefficient (HTC) and the interfacial area density (IAD).

### 1.1 Background

Condensation induced water hammers are classified as water hammers that occur when subcooled liquid is brought into contact with saturated steam. These transients start with direct contact condensation of saturated steam on subcooled liquid which results in increase of Kelvin-Helmholtz instability [6]. This leads to formation of slug flows with steam bubbles entrapped by subcooled liquid. Rapid condensation of the entrapped steam bubbles will result in a low pressure void surrounded by liquid that will rush to fill in. The resulting collision of the liquid will generate a pressure spike that propagates along the system. A schematic representation of the condensation induced water hammer can be seen in Figure 1.1

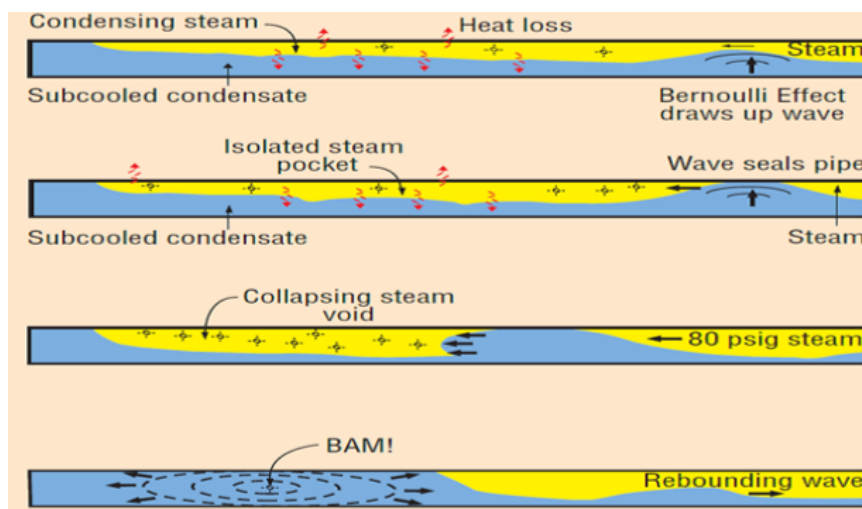


Figure 1.1: Schematic representation of CIWH phenomenon [1]

A similar scenario like this can occur during Loss of Coolant Accident (LOCA) event in nuclear power plants. During LOCA event, subcooled water is injected into a primary power plant loop, counter-currently to steam exiting the reactor by Emergency Core Cooling System (ECCS). Under certain conditions, this might lead to a CIWH. These transients might also occur in the operation of steam pipelines and solar thermal plants [2].

## 1.2 Objective

The main objective of this thesis work is to model DCC phenomenon and study the performance of the condensation models. Initially, a literature survey is conducted to study how this phenomenon can be modeled and what condensation models can be used. Ansys Fluent is used to simulate DCC and condensation models based on Surface Renewal theory are used. The simulation results are compared against experimental results from LAOKOON facility.

## 1.3 Literature Survey

Nuclear industry primarily uses 1-D system codes like RELAP5 [32] or TRACE [33] to conduct various safety assessment studies. These system codes are computationally inexpensive and can perform full system analysis employing relatively coarse computational grids and are developed using two-fluid six-equation approach. Equations describing mass balance, momentum conservation and energy are solved for both phases individually. Both phases are coupled using the interfacial momentum exchange in momentum conservation equations. Even though the system codes achieve a good resolution of results, in order to understand the full system behaviour, local and accurate behaviour are needed and this cannot be studied using these codes. Computational Fluid Dynamics (CFD) can be used to accurately study the local physical behaviour, however they are computationally very expensive. An accurate tracking of the two phase interface is necessary to study the DCC phenomenon. Among the available approaches, the most important techniques which can be used to accurately track interface are: VOF Method [3], Level Set Method (LSM) [4] and front-tracking method [5]. The main advantage of VOF method over LSM is its ability to conserve mass [6]. This makes VOF method more popular to track interfaces even though LSM has the capability to track the interface better. In VOF, a single velocity field is shared among both phases, this makes it inappropriate for the description of polydispersed flows with a large density ratio between the two phases. In order to achieve a sharp interface, a fine resolution is necessary near the interface, but a sharp interface will result in numerical instabilities. So, it is always a trade off between the sharpness of the interface and numerical stability. A two-fluid model with suitable algorithms to track the interface might be an alternative to pure interface tracking methods, which fail when the characteristic length of the interface becomes less than the grid size. However, the two phase interface cannot be tracked accurately because of the assumption of interpenetrating phases in the

two-fluid model.

The investigation of interfacial heat and mass transfer during phase change and the effect of turbulence near the interface still remain a challenge in CFD. Inclusion of phase change in two-phase flows will introduce additional sources into the conservation equations. Source terms representing mass transfer are introduced in mass conservation equation and energy source term representing heat transfer is introduced in the energy equation. The energy source term ( $Q$ ) is calculated by multiplying mass transfer ( $\dot{m}$ ) with latent heat ( $h_{lv}$ ).

$$Q = \dot{m}h_{lv}. \quad (1.1)$$

Hughes and Duffey [7] developed a method to calculate the interfacial heat and mass transfer using surface renewal theory. In this method, the liquid turbulence is directly correlated to the calculation of the heat transfer coefficient.

The surface renewal theory [8] predicts the amount of mass transfer from the liquid turbulent properties. The amount of mass transfer is controlled by the surface renewal time. The surface renewal time is calculated using the turbulent length and velocity scales and the heat transfer coefficient depends on the surface renewal time.

$$\dot{m} = \frac{HTC * (T_{sat} - T_l) * IAD}{h_{lv}}, \quad (1.2)$$

where IAD and HTC are the interfacial area density and the heat transfer coefficient. IAD is calculated as the ratio of interface area and the volume of geometry

$$IAD = a_i = \frac{A_{interface}}{V}, \quad (1.3)$$

where A and V are the interface area and volume, respectively.

The Hughes and Duffey correlation uses the surface renewal time based on the Kolmogorov scales to predict the heat transfer coefficient at the two phase interface as

$$HTC_{HD} = 2\rho_l C_{pl} \left( \frac{\alpha_{tl}}{\pi} \right)^{\frac{1}{2}} \left( \frac{\epsilon}{\nu_l} \right)^{\frac{1}{4}}. \quad (1.4)$$

Ceuca and Macián-Juan [30] implemented the Hughes and Duffey correlation with a VOF approach to study DCC phenomenon in ANSYS CFX. They also implemented the Shen correlation [9], which is also based on surface renewal theory for the calculation of the heat transfer coefficient. HTC in the Shen correlation is calculated as

$$HTC_{shen} = 0.794\lambda_l L_t^{-\frac{1}{3}} \left( \frac{V_t}{\nu_l} \right)^{\frac{2}{3}} (Pr_l)^{\frac{1}{2}}. \quad (1.5)$$

The Shen correlation considers large eddies for calculation of surface renewal time. This results in a lower heat transfer coefficient compared to the Hughes and Duffey correlation. Ceuca and Macián-Juan achieved better results with Shen correlation. The choice of using constant surface renewal time thought the simulation is questioned by Fan L.T, Shen B.C, and Chou S.T [10]. They calculated the surface

renewal time using stochastic population balance. Štrubelj et al. [11] implemented the Hughes and Duffey correlation with two-fluid model in NEPTUNE\_CFD code to study DCC.

Coste [12][13] introduced a method for friction and turbulence around large interfaces in simulations with a two-fluid model. The large interface is made of three layers and the thickness of each layer is one cell. An anisotropic friction model is implemented in large interface along with a two-fluid model in the NEPTUNE\_CFD code. Štrubelj et al. [14] compared Hughes and Duffey correlation with the large interface model and achieved better result with the large interface model. Szijártó [15] studied condensation in horizontal pipes using four different methods: Lee numerical iteration technique [16], Surface renewal theory correlation, Direct solution of the heat flux balance equation and Phase field theory based equation [17]. The Lee model imposes a boundary condition that the two phase interface is at the saturation temperature. The mass transfer is introduced in the interface cell such that the boundary condition is reached through iteration. The iteration speed is governed by a coefficient and should be tuned for each simulation. Mass transfer is calculated in the Lee model as

if  $T_l > T_{sat}$  (evaporation)

$$\dot{m} = c * \alpha_l \rho_l \frac{T_l - T_{sat}}{T_{sat}}, \quad (1.6)$$

and if  $T_v < T_{sat}$  (condensation)

$$\dot{m} = c * \alpha_v \rho_v \frac{T_{sat} - T_v}{T_{sat}}. \quad (1.7)$$

A sharp interface is necessary to study DCC phenomenon. VOF approach is chosen considering its ability to track a sharp interface. Even though Lee model produces accurate results, the coefficient ( $c$ ) should be tuned for different simulations. So it is decided to study the condensation models based on surface renewal correlations. They are explained in detail in chapter 2.

# 2

## Theory

This section provides a description of the two-phase flow dynamics. It also discusses different techniques for numerical simulations of two-phase flows and the governing equations used. Further, it describes about surface renewal theory and the condensation models which are developed based on the surface renewal theory. This section also contains the description of various implementations that are used in present work and the experimental facility used for validation of results.

### 2.1 Two-Phase flows

In fluid mechanics, simultaneous flow of several phases is called multiphase flow. Studying and understanding the complex nature of multiphase flows is very important in many industries, particularly energy-related industries. Two-phase flow is a simple case of multiphase flows where two phases flow simultaneously. Two-phase flows can be solid-liquid, gas-liquid, liquid-liquid and gas-solid. Two-phase flow consisting of gas and liquid can be seen widely in nuclear industry. Accurate modelling of two-phase flows can play a vital role during the design and safety assessment of new equipment. The description of phase distribution of gas and liquid in a flow channel is very important for accurate modelling of these flows. The heat transfer coefficient, interfacial area density, and pressure drops are closely related to local flow structures of the two-phase flow. Flow regime maps can be used to predict the local flow structure in a channel. These maps determine the flow structure based on the variables like phase velocities, mass fluxes, void fractions, etc [18]. The commonly occurring flow structures are defined as two-phase flow patterns. In general, two-phase flow regimes in horizontal channels show a non-symmetrical pattern which is due to the effect of gravity on fluids with different densities [19]. This leads to stratification of liquid on the bottom of the channel with gas on top. Flow patterns for co-current flow of liquid and gas in a horizontal tube are shown in Figure 2.1 and are categorized as follows [19]:

- **Bubbly flow** - In bubbly flow, gas bubbles are dispersed in the liquid with a high concentration in the upper half of the channel due to buoyancy. The bubbles tend to disperse uniformly in the channel if shear forces become dominant. Typical features of this flow are moving and deformable interfaces of bubbles in time and space domains and complex interactions between the interfaces, and also between the bubbles and the liquid flow. In horizontal flows, bubbly flow typically occurs only at high mass flow rates.

- **Stratified flow** - In stratified flow the two phases are completely separated with a smooth interface. The liquid phase is present at the bottom of the channel with gas on top. This regime occurs at low liquid and gas velocities.
- **Wavy flow** - Increasing the gas velocity in stratified flow will lead to formation of waves on the liquid surface which will move in the direction of the flow. The amplitude of the waves depends on the relative velocity of the phases.
- **Plug flow** - If the gas velocity is increased further, the amplitude of the waves increases and results in entrapment of gas bubbles. This regime has liquid plugs that are separated by elongated gas bubbles. The diameter of the elongated bubbles is smaller than the channel such that the liquid phase is continuous along the channel. This regime is also referred to as *elongated bubble flow*
- **Slug flow** - Slug flow is similar to plug flows, but the main difference is the diameter of the elongated gas bubbles. In slug flows, the diameter of the elongated bubbles become similar in size to channel height. The liquid slugs can also be described as large amplitude waves.
- **Annular flow** - If the gas velocity is increased even further, annular flow will develop in which the liquid flow is mostly through annular zone. The gas phase will flow through the center of the channel. The interface between liquid and gas contain small amplitude waves and the gas phase may contain liquid phase in the form of droplets.
- **Dispersed flow** - If one phase is dispersed in a continuous phase, the flow regime is called dispersed flow. Bubbly flow is an example of dispersed flow where gas bubbles are dispersed in the liquid.

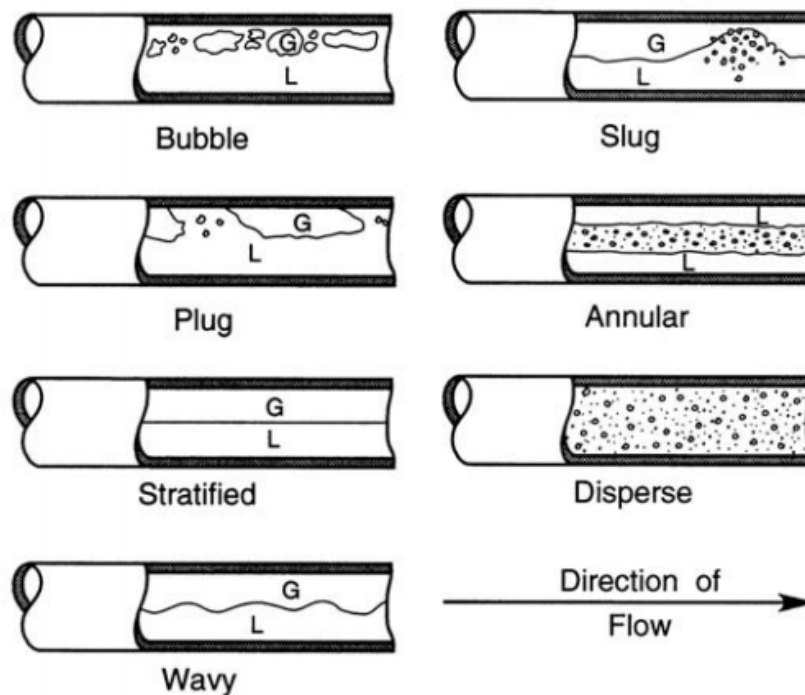


Figure 2.1: Two-phase flow patterns in horizontal flow [29]

## 2.2 Direct contact condensation

Direct contact condensation (DCC) is a phenomenon where saturated steam condenses on subcooled liquid. This phenomenon can appear with any liquid and its vapor. DCC is a commonly occurring phenomenon in many industries and has particular importance in nuclear industry. DCC can act as driving force to a violent condensation phenomenon called condensation induced water hammer. The local depressurization which is caused by DCC results in the acceleration of liquid to fill the void resulted by condensation of steam. This enhances the Kelvin-Helmholtz instability and results in occurrence of slug flow with steam bubbles entrapped by subcooled liquid. The sudden collapse of these steam bubbles will result in condensation induced water hammer (CIWH).

The key parameters that describe the DCC phenomenon are the heat transfer coefficient (HTC) and the area in contact with the two phases (IAD). A reliable prediction of both parameters is necessary to accurately model DCC. In this work surface renewal theory is used for computation of HTC. The surface renewal theory directly correlates the calculation of HTC to the liquid turbulence properties. They are further explained in section 2.4.

## 2.3 Numerical Simulation of Two-Phase flow

The equations that describe the physics of two-phase flow are all based on conservation laws for mass, momentum and energy. Numerical simulations of two-phase flows are in general computationally more expensive than single phase flows because of the presence of two phases that need to be tracked along the flow. It is also necessary to model the interaction between the phases at the interface. Several models are developed based on the physics of the flow and the level of the information i.e. accuracy, needed. In this work two models, the two-fluid model and Volume of fluid Model (VOF) which are based on Euler-Euler approach are studied. They are presented in detail in the next section.

### 2.3.1 Two-Fluid Model

In two-fluid model, Eulerian conservation equations are derived assuming that two phases are interpenetrating continua and are represented by averaged conservation equations. By introducing the phase fraction  $\alpha$  into the equations, two phases are allowed to co-exist at a point. Conservation equations are written for each phase and phase interaction is handled using the interfacial momentum transfer term in the momentum equation.

Governing equations of a transient two-fluid model for the phase q are written as below:

1. Phase mass conservation:

$$\frac{\partial(\alpha_q \rho_q)}{\partial t} + \nabla \cdot (\alpha_q \rho_q \vec{U}_q) = \Gamma_q, \quad (2.1)$$

where  $\alpha_q$ ,  $\rho_q$  and  $\vec{U}_q$  represent volumetric phase fraction, density and velocity of phase q, respectively.

$\Gamma_q$  represents the source/sink term accounting for phase change.

$$\Gamma_q = \dot{m} a_i, \quad (2.2)$$

where  $\dot{m}$  and  $a_i$  are the interfacial mass transfer and interfacial area density, respectively.

The interfacial area density is computed according to:

$$a_i = \frac{A_{interface}}{V}, \quad (2.3)$$

where V is total volume of the considered geometry entity and A is the interface area.

### 2. Phase Momentum Conservation:

$$\frac{\partial(\alpha_q \rho_q \vec{U}_q)}{\partial t} + \nabla \cdot (\alpha_q \rho_q \vec{U}_q \vec{U}_q) = -\alpha_q \nabla p + \nabla \cdot (\alpha_q (\tau_q + \tau_q^t)) + \alpha_q \rho_q \vec{g} + S_M, \quad (2.4)$$

where interfacial momentum transfer term  $S_M = \Gamma_q \vec{U}_{qi} + M_q$  and  $\tau_q, \tau_q^t$  are the molecular and Reynolds stress tensors,  $p$  is the averaged pressure field.

$M_q$  represents the interfacial momentum exchange and is modelled using the lift, drag, virtual mass and other forces, like the Basset force.

### 3. Phase Energy Conservation:

$$\frac{\partial(\alpha_q \rho_q h_q^{tot})}{\partial t} + \nabla \cdot (\alpha_q \rho_q h_q^{tot} \vec{U}) = \alpha_q \frac{\partial p}{t} + \alpha_q \rho_q \vec{g} \vec{U}_q - \nabla \cdot [\alpha_q (\vec{q}_q + \vec{q}_q^t)] + S_E, \quad (2.5)$$

where  $S_E = \Gamma_q h_q^{tot} + q_{qi}'' a_i + q_{wq}'''$  and  $h_q^{tot}$  represents the sum of the phase-averaged enthalpy for phase q and its kinetic energy  $\frac{U_q^2}{2}$ .

The variables  $\vec{q}_q$  and  $\vec{q}_q^t$  are molecular and turbulent heat flux vectors respectively,  $q_{qi}'' a_i$  and  $q_{wq}'''$  are the interfacial heat transfer and the heat transfer from the wall to the fluid respectively.

The two-fluid model can be used for all regimes including separated, dispersed and intermediate since the topology of the flow is not prescribed. However, modelling of interfacial momentum transfer term is different because it depends on the exact nature of the flow. Predictive capabilities of the two-fluid model depend heavily on both interfacial momentum transfer term and a two-phase turbulence model.

The assumption of interpenetrating phases will result in the loss of exact shape and position of the interface. Although this is not a shortcoming in many two-phase problems, there are situations where the phases are sharply separated and knowledge about the interface is crucial. In our case, subcooled water and steam are flowing concurrently in a pipe and clearly one needs to know the characteristics of the steam-water interface to estimate the condensation rate taking place there.

### 2.3.2 Volume of Fluid Model

The Volume of Fluid Model was first introduced by Hirt and Nichols [20]. It is widely used in simulations where characteristics of interface is important. Conservation equations are developed on the assumption that two phases are not interpenetrating. Governing equations are solved using the volume fraction in a cell. Summation of volume fraction  $\alpha_q$  of all phases in a cell is unity.

$$\sum_{q=1}^{\infty} \alpha_q = 1 \quad (2.6)$$

Consider a vapour bubble in water as shown in Figure 2.2. In the figure  $\alpha_q = 0$  represents water region and  $\alpha_q = 1$  represents vapour region. If the volume fraction is  $0 < \alpha_q < 1$  then the cell represents an interface region, as shown in Figure 2.2. In the interface region liquid and vapour will co-exist.

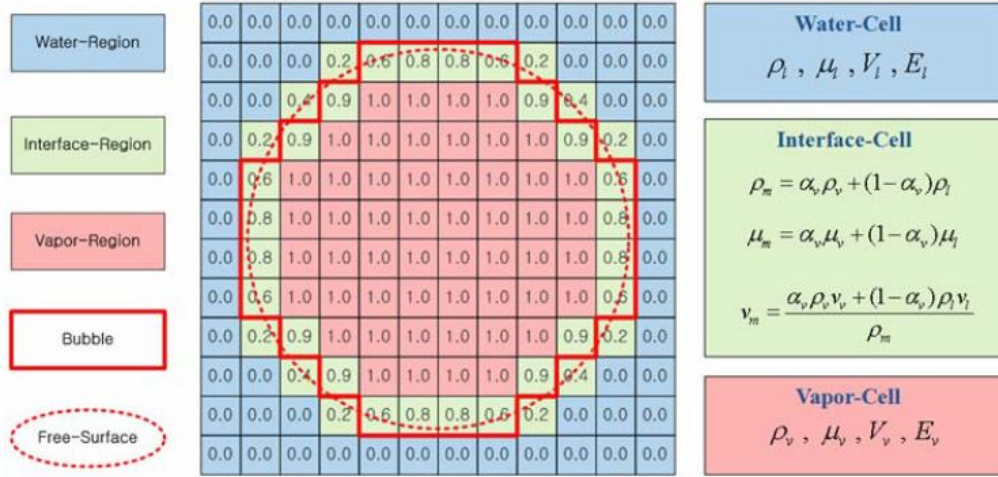


**Figure 2.2:** Volume fraction and properties in each cell [21]

All properties in VOF that are shared by phases are calculated using the volume fraction contributions of each phase in the cell. For example, if we are tracking the volume fraction of vapour in the above example, then any property  $P$  in a cell is tracked as below,

$$P = \alpha_v P_v + (1 - \alpha_v) P_l. \quad (2.7)$$

The tracking of interface is accomplished by the solution of a continuity equation for the volume fraction of one of the phases. For the  $q^{th}$  phase, this equation has the following form

$$\frac{\partial(\rho_1 \alpha_q)}{\partial t} + \nabla \cdot (\rho_1 \alpha_q \vec{U}) = \Gamma_{\alpha_q}, \quad (2.8)$$

where  $\Gamma_{\alpha_q}$  represents the source/sink term accounting for phase change.

A single momentum equation corresponding to typical RANS approach is solved throughout the domain and the resultant velocity field is shared among all phases.

$$\frac{\partial(\rho\vec{U})}{\partial t} + \nabla \cdot (\rho\vec{U}\vec{U}) = -\nabla p + \nabla \cdot (\mu\nabla\vec{U}) + \rho\vec{g} + f_i, \quad (2.9)$$

where  $U$  is treated as the mass-averaged variable, and

$$U = \frac{\alpha_1\rho_1U_1 + \alpha_2\rho_2U_2}{\rho}, \quad (2.10)$$

where subscripts 1 and 2 corresponds to two different phases.

In the momentum equation,  $f_i$  represents momentum source term due to surface tension. It is only active at the interface.

The energy equation, also shared among the phases is shown below

$$\frac{\partial(\rho h^{tot})}{\partial t} + \nabla \cdot (\rho h^{tot}\vec{U}) = \nabla \cdot (k_{eff}\nabla T) + S_E, \quad (2.11)$$

where  $S_E$  accounts for heat transfer at the interface.

VOF is suitable for describing two-phase problems, where the characteristic length of the interface shape is larger than the grid size of the computational domain. A sharp interface is required to obtain accurate results. But, a sharp interface will result in numerical instabilities because of sudden change in properties across interface. This can be avoided by smearing the interface across few cells.

## 2.4 Surface Renewal Theory

The concept of surface renewal theory was first introduced by Higbie[8] describing the rate of absorption of a pure gas into a still liquid. It is based on the concept of extremely small, but finite liquid elements migrating to the two-phase interface where they interact with the gaseous phase for a certain duration before being replaced with a fresh fluid element. This migration and removal of fluid elements is induced by the turbulent eddies in liquid flow. Mass transfer from one phase to other is governed by unsteady molecular diffusion and is controlled by the time liquid elements are exposed to interface. This exposure time is called surface renewal time and is related to the characteristic eddy length scale  $L_t$  and velocity scale  $V_t$ , by

$$SRT = \frac{L_t}{V_t}. \quad (2.12)$$

The contact times of these fluid elements arriving at the interface are assumed to be uniformly distributed. Some modified versions of surface renewal theory assumed that these contact times are completely random [22], or exponentially distributed [10]. The interfacial heat transfer models derived from this approach directly correlate the calculation of heat transfer coefficient to the turbulence properties of the

flow. In this approach, the effects of wall and the interfacial shear and eddy diffusivity distribution on heat and mass transfer are directly derived from the momentum transfer. The difficulty in surface renewal theory based models is choosing appropriate length and velocity scales of turbulent eddies. Choice of these scales will affect the surface renewal time which in turn affects the overall mass transfer rates.

### 2.4.1 Hughes and Duffey model

Hughes and Duffey's model [7] extended the applicability of surface renewal theory to the case of interface mass and heat transfer in shallow flows, where the presence of both the interface and wall shear had to be included. The mass transfer coefficient in stratified flows is dependent on the shear due to the turbulent wind blowing over the rough and wavy water surface. This is because the momentum transfer generates turbulence in the water that transports gas-laden flow from the surface into the bulk liquid below [23]. Based on this, the authors postulated that the turbulent energy flux in the air is in equilibrium with the turbulent dissipation in the liquid through the action of interfacial shear. They considered Kolmogorov scales to include the presence of wave breaking and foaming [24] and also considered that these scales are mainly responsible for transfer of energy. Choosing of Kolmogorov scales will result in a shorter surface renewal time which in turn results in more energy transfer rate between the interface and liquid bulk.

The heat flux at gas liquid interface is calculated as proposed by Banerjee[25] as

$$q_{iGL} = 2\rho_l C_{pl} \left( \frac{\alpha_{tl}}{\pi} \right)^{\frac{1}{2}} \left( \frac{1}{t_{rp}} \right)^{\frac{1}{2}} (T_{sat} - T_l), \quad (2.13)$$

where  $\alpha_{tl}$  is the thermal diffusivity and  $t_{rp}$  is the surface renewal time. The heat transfer coefficient is

$$HTC = \frac{q_{iGL}}{T_{sat} - T_l} = 2\rho_l C_{pl} \left( \frac{\alpha_{tl}}{\pi} \right)^{\frac{1}{2}} \left( \frac{1}{t_{rp}} \right)^{\frac{1}{2}}. \quad (2.14)$$

Surface renewal time is determined by the Kolmogorov length and velocity scales and the dissipation of energy in the liquid as

$$L_t = \left( \frac{\nu_l^3}{\epsilon} \right)^{\frac{1}{4}}, \quad V_t = (\nu_l \epsilon)^{\frac{1}{4}}, \quad (2.15)$$

rearranging and replacing the value of  $t_{rp}$  in equation 2.14 will lead to the final version of the HTC as,

$$HTC = 2\rho_l C_{pl} \left( \frac{\alpha_{tl}}{\pi} \right)^{\frac{1}{2}} \left( \frac{\epsilon}{\nu_l} \right)^{\frac{1}{4}}. \quad (2.16)$$

### 2.4.2 Shen et al. model

The formulation of Shen et al. model [9] is similar to the Hughes and Duffey model with a small change in the choice of the turbulent scales. This model considers that the larger eddies are mainly responsible for the transfer of energy between the

interface and liquid bulk. This model uses slightly modified Kolmogorov velocity scale and length scale of standard  $k - \epsilon$  model as shown below,

$$L_t = c_\mu \frac{k^{\frac{3}{2}}}{\epsilon}, \quad V_t = (c_\mu)^{\frac{1}{2}} (\epsilon \nu_l)^{\frac{1}{4}}. \quad (2.17)$$

The final version of HTC based on this model is taken from [28] as

$$HTC = 0.794 \lambda_l L_t^{-\frac{1}{3}} \left( \frac{V_t}{\nu_l} \right)^{\frac{2}{3}} (Pr_l)^{\frac{1}{2}}, \quad (2.18)$$

where  $Pr_l$  is the prandtl number and  $\lambda_l$  is the thermal conductivity of liquid. Considering this scales of length and velocity will result in a higher surface renewal time compared to Hughes and Duffey model. This will result in lower HTC and less energy transfer rate between the interface and liquid bulk.

## 2.5 Description of LAOKOON experimental facility

The LAOKOON experimental facility was built at Technical Universität München (TUM) by Goldbrunner et al. [26] for the experimental investigation of DCC over subcooled water. The experimental setup consists of a rectangular channel  $L = 1200 \text{ mm} \times H = 106 \text{ mm} \times W = 79 \text{ mm}$  with two separate inlets for water and vapor phase. Channel cross section of the LAOKOON experimental facility with two separate inlets and outlets is shown in Figure 2.3.

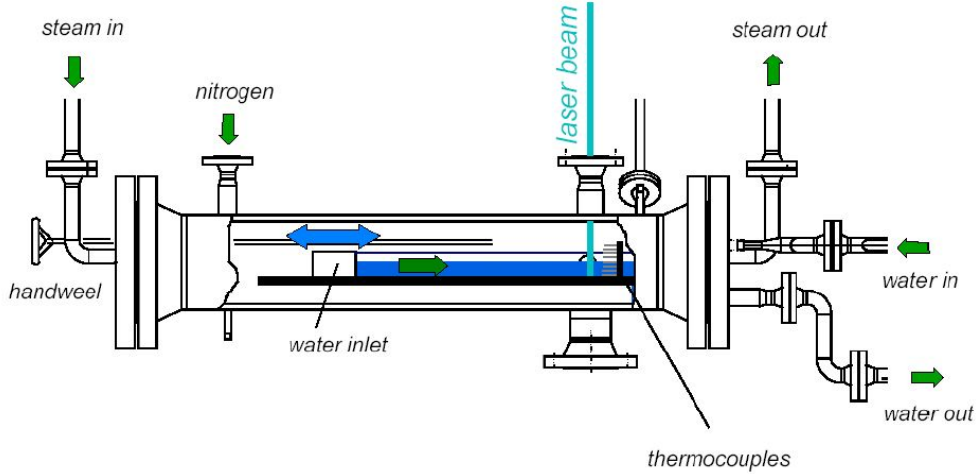


**Figure 2.3:** LAOKOON experimental set up [26]

The set-up is used to develop a steady quasi-2D pattern with subcooled water flowing along the bottom of the channel and saturated dry steam on top of the liquid with nearly adiabatic wall conditions. The channel walls are thermally insulated to ensure adiabatic wall conditions, as shown in Figure 2.4.

Careful design of inlet and outlet of water ensured a horizontal free surface throughout the channel. A transparent window allowed for visual inspection of possible

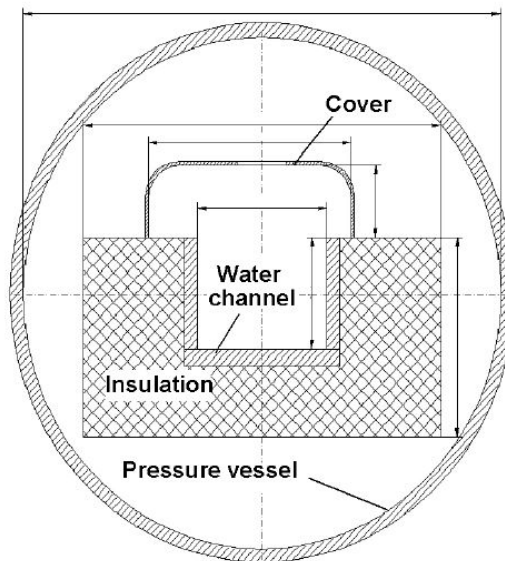


**Figure 2.4:** Flow wise cross section of LAOKOON experimental set-up [27]

waves on water surface. The vertical temperature profile in the water is measured using 12 micro, NiCr-Ni PT100 thermocouples which are placed at a distance of 790 mm from the inlet. Experiments were done with and without non-condensable gas in the vapor phase. The steam inlet is supplied with saturated dry steam at the temperature corresponding to the measured pressure level in the channel which is 6.97 bar. The pressure and water levels in the channel, steam and water flow rates at inlet, inlet water temperature are provided. All the given parameters are listed in Table 2.1.

Parameter	Value
Inlet water velocity[m/s]	0.28
Inlet steam velocity[m/s]	3.20
steam inlet temp[k] ( $T_{sat}$ )	437.93
water inlet temp[k]	310.2
Height of water level[m]	0.031
water turb. intensity	8%
steam turb. intensity	not available
Pressure [bar]	6.97
Water Reynolds number	28082
Steam Reynolds number at inlet	51051

**Table 2.1:** Parameters of LAOKOON experimental set-up [27]

No waves are visually observed during the course of experiment. The specially arranged measurements confirmed that the flow in the duct was two-dimensional, with negligible influence of the walls [27]. The temperature rise in water because of latent heat of condensation is observed during the experiment. The temperature data along the thermocouple line is presented in Table 2.2.

Water level in [m]	Temperature in [k]
0.004	310.94
0.008	310.48
0.012	311.31
0.016	313.14
0.02	316.42
0.024	322.26
0.026	331.79
0.028	354.73
0.03	411.97
0.031	435.67
0.034	434.77
0.036	435.74

**Table 2.2:** Temperature data near thermocouple line [27]

## 2.6 Implementation

ANSYS Fluent is used to simulate the case and condensation model is included into VOF equations using the User-Defined functions (UDF). A UDF, is a C function which can be dynamically loaded with the solver. These UDFs are mainly used to enhance the capabilities of ANSYS Fluent solver. They are defined by using DEFINE macros and are coded using additional macros and functions provided by ANSYS Fluent. This additional macros and functions can access Fluent solver data and can be used to perform various other tasks [28]. Fluent also provides additional tools like User-Defined Memory and User-Defined Scalar which can be used along with User-defined functions.

A User-Defined Memory (UDM) can be used to store the variables and call them during the calculation using macros. This can be activated by allocating appropriate number of memory locations in the UDM dialog box in ANSYS Fluent. A maximum of 500 memory locations can be used in Fluent and system requirements increase as the number of memory locations increases.

A User-Defined Scalar (UDS) can be used to solve an additional scalar transport equation in the domain along with other scalar equations. They can be used for both single and multiphase flows. A maximum of 50 UDS can be used in a calculation. The general scalar transport equation which can be used in Fluent with the four terms transient, flux, diffusivity and source is shown in equation 2.19 as

$$\frac{\partial(\rho\phi)}{\partial t} + \nabla(\rho\vec{U}\phi - \Gamma\nabla\phi) = S_\phi, \quad (2.19)$$

where  $\rho$ ,  $\Gamma$ ,  $S_\phi$ , are density, diffusion coefficient and source term respectively.

The following UDFs are used for implementing the condensation model in Fluent

- DEFINE\_ADJUST: to calculate the interfacial area density and store in an UDM.

- DEFINE\_SOURCE: three DEFINE\_SOURCE macros are used to calculate source terms in continuity and energy equation.
- DEFINE\_DIFFUSIVITY: to define diffusivity when UDS is used.

In addition to these, several UDM locations are used to store the variables and are later used for post processing. One UDS is also used when the smearing function is implemented. In order to improve the convergence and stability of the code, additional functions like temporal relaxation, turbulence damping and ramp up function are implemented along with the condensation model.

### 2.6.1 Temporal relaxation

Introducing source terms only at the interface resulted in large pressure fluctuations and made the code very unstable. To increase the stability of the code, a time dependent relaxation of source terms is implemented. Instead of passing the actual mass transfer and heat transfer, an average of six previous time steps was passed. UDMs are used to store previous time step values and called in the current time step to calculate the average. This allowed to use higher time step and increased the stability of the code. Implementation of this relaxation can be seen in the below equation,

$$m_{(t)} = \frac{(m_{(t)} + m_{(t-1)} + m_{(t-2)} + m_{(t-3)} + m_{(t-4)} + m_{(t-5)})}{6} \quad (2.20)$$

where m, t are mass transfer and time step respectively.

### 2.6.2 Turbulence Damping

High velocity gradients at the interface between two phases will result in high turbulence generation when differential eddy viscosity models like the  $k - \epsilon$  and  $k - \omega$  models are used without any special treatment of the free surface [28]. This turbulence will result in waves which are not desirable in this case. Hence, turbulence damping is required at the interface to model such flows correctly. Turbulence damping is implemented in Fluent by introducing a source term to the  $\omega$ -equation [28].

$$S_i = A_i \Delta n \beta \rho_i \left( \frac{B 6 \mu_i}{\beta \rho_i \Delta n^2} \right)^2 \quad (2.21)$$

where,

- $A_i$  = Interfacial area density for phase i
- $\Delta n$  = cell height normal to interface
- $\beta$  =  $k - \omega$  model closure coefficient of destruction term, which is equal to 0.075
- $B$  = Damping factor
- $\mu_i$  = Viscosity of phase i
- $\rho_i$  = Density of phase i.

The interfacial area density is calculated as

$$A_i = 2\alpha_i |\nabla \alpha_i| \quad (2.22)$$

where,

$$\begin{aligned} \alpha_i &= \text{volume fraction for phase } i \\ |\nabla\alpha_i| &= \text{magnitude of gradient of volume fraction.} \end{aligned}$$

The default value for damping factor B is 10.

### 2.6.3 Calculation of Interfacial area density

Interface is well resolved with the compressive discretisation of volume fraction equation and is typically restricted to three or four grid cells. There is no direct way of calculating interfacial area density within VOF methodology and should be modelled. The modelled interfacial area density should have a maximum at the middle of the interface and should approach to zero moving away from center of interface. One more requirement for the model is the normalizing condition which is the volume integral of the area density must be equal to the real surface area. This means that the integration of area density along a normal to the surface should be equal to unity

$$\int_{-\infty}^{\infty} a_i dn = 1.$$

A model which satisfies this condition, calculates the interfacial area density as the absolute value of volume fraction gradient

$$a_i = |\nabla\alpha_l| = \frac{\partial\alpha_l}{\partial n},$$

where  $\alpha_l$  is the liquid volume fraction and n is directed to bulk liquid phase.

### Built in limitations

The following limitations are implemented to avoid numerical diffusion of mass transfer and to restrict heat and mass transfer only to the interface,

- cut off for volume fraction is implemented , vof cut-off = 0.0001.
- heat and mass transfer are calculated only in cells where (vof cut-off) <  $\alpha_l$  < (1-vof cut-off), i.e., only at interface.
- heat and mass transfer is only calculated if  $IAD(A_i) > 1$  and  $T_{sat} - T_l > 0.00001$ .

# 3

## Geometry and Mesh

In this section, simulation setup and the geometry used are described. First, the geometry and the computational domain are described, then in section 3.3 the simulation setup is presented.

### 3.1 Domain Geometry

The LAOKOON experimental setup is used for simulation of DCC. Considering the negligible effect of side walls, only a 2D slice of the geometry is used for the simulations. A schematic representation of the geometry used is shown in Figure 3.1. The length of the channel is increased from 990 mm to 1000 mm to decrease the effect of outlet at the thermocouple location. The height of the channel is considered as 106 mm in the calculation and differs from the ECORA project [27] where height is 128 mm. This is because, in the ECORA project the author considered channel cover as the top of the channel instead of actual channel height.

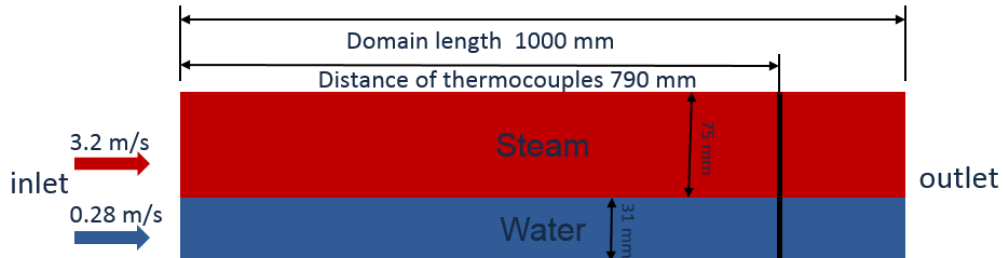


**Figure 3.1:** Flow wise cross section of LAOKOON experimental set-up [26]

### 3.2 Grid Generation

A two-dimensional mesh is generated using ANSYS ICEM CFD. The mesh is refined close to the steam-water interface and walls in vertical direction. The inlet of the channel is divided into two sections for steam and water according to the water level. Two meshes are generated, a coarse mesh with 23000 cells and a fine mesh with 62000 cells. Resolution at the interface is 0.33 mm for the two meshes in the y direction. The fully developed mesh with refinement close to the interface can be seen in Figure 3.2

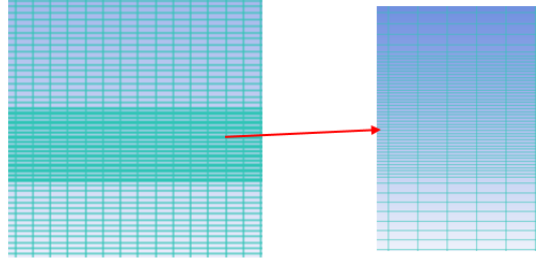


**Figure 3.2:** Mesh generated for LAOKOON facility

### 3.3 Case setup

Ansys Fluent is used for solving the governing equations. The simulations are run in transient mode until steady state conditions are reached. The velocity inlet and pressure outlet boundary conditions are used at inlet and outlet of the channel. The top and bottom of the channel are treated as adiabatic walls. A compressive scheme [29] and implicit VOF solver is used to achieve a well resolved interface. Turbulence modelling is implemented using  $k-\omega$  SST model. The  $k-\omega$  model is mainly chosen because turbulence damping is only implemented with that model in Ansys Fluent. Turbulence damping with a coefficient of 10 is used in the calculations. Coupled scheme is used to achieve the pressure-velocity coupling. The pressure is discretized using PRESTO! algorithm and the second order upwind scheme is used for the remaining equations. Constant thermo-physical properties are used to decrease the computation time. The material properties used for both phases are listed in Table 3.1

Property	Liquid	Steam
Temperature $T_{sat}$ [K]	310.2	437.93
Density $\rho$ [kg/m <sup>3</sup> ]	996.77	3.67
Viscosity $\mu$ [kg/ms]	8.4e-04	1.45e-05
Thermal conductivity $\lambda$ [W/mK]	0.6109	0.03389
Specific heat $C_p$ [J/kg-K]	4179	2543

**Table 3.1:** Material properties used in LAOKOON experiment [26].

Condensation model is introduced into VOF equations using UDFs. Total of four UDFs are used in the calculation. UDM locations are used to implement the temporal relaxation. The initial temperature, velocity and water level are set in the channel using Patch option in Fluent. Initially, a transient calculation without the energy equation and condensation model is run, until the convergence is reached. Once the flow is developed, the velocity and pressure profile is saved along a vertical line and these values are set as inlet and outlet conditions. This procedure is iterated for couple of times to get a suitable outlet pressure to maintain the water level in the channel without any waves and reverse flow. This procedure also allowed to obtain a near perfect stratified flow with very small waves at the inlet. This procedure was mainly done because the height of the water level is imposed at the outlet in the

LAOKOON experiment, also to obtain a perfect stratified flow as in the experiment. Various geometrical configurations like having two separate outlets for steam and water, having a tank at the outlet are tried but none of them were able to maintain the water level as in the experiment without any waves.

The resulted velocity and pressure profiles are further used as inlet and outlet boundary conditions for the calculation with condensation models. A transient calculation without condensation model is run with a time step of 5e-04 s using the obtained velocity and pressure profiles as inlet and outlet boundary conditions. This is run until the flow is developed (t=1.5 s) before switching on the condensation model.

Introducing the source terms into the equations when condensation model is switched on resulted in large pressure fluctuations and made the code unstable. These pressure fluctuations might be because of the following reasons

- introducing large source terms only at the interface
- existence of a large gradient in source terms introduced between time steps
- existence of a large gradient in source terms introduced in the domain.

In order to avoid these pressure fluctuations, temporal relaxation which is discussed in section 2.6.1 is used in all the simulations. A smearing function using a scalar transport equation is also tried in order to smear the source term values across few cells, but this again resulted in small pressure fluctuations. This method also required to decrease the time step to  $10^{-5}$  s. Turbulence damping is also implemented in all the simulations to obtain stratified flow. A ramp function is also implemented in the code to make it more stable. Mass transfer is ramped slowly for two seconds to reach the actual value. Table 3.2 shows all the cases which are simulated.

Simulation Name	Mesh	Condensation model used
case-1	coarse	Hughes and Duffey [7]
case-2	fine	Hughes and Duffey [7]
case-3	coarse	Shen et. al [9]
case-4	coarse	Hughes and Duffey with modified energy source term

**Table 3.2:** Cases simulated in this work

Case 4 has a modified energy source term compared to the actual source term. The actual source term is calculated by multiplying the mass transfer with the latent heat. In reality, heat is removed from the gas phase and added to liquid phase. But this cannot be implemented exactly, since only one energy equation is solved in VOF. In order to avoid this problem, the energy source term is slightly modified as below

$$\text{energy source term} = \text{mass transfer} * (h_{\text{steamsat}} - h_l),$$

where  $h_{\text{steamsat}}$  and  $h_l$  are saturated steam enthalpy and enthalpy of liquid coming into the channel.



# 4

## Results and discussion

In this section, the results from the different simulations are presented. As discussed in the previous section, initially a transient calculation without the condensation model and the energy equation is solved to obtain appropriate velocity and pressure profiles for boundary conditions. The proper outlet pressure prevented reverse flow and maintained water level in the channel. Turbulence damping is introduced at the interface to obtain a smooth stratified flow pattern in the channel. Small waves are observed close to the inlet. Figure 4.1 shows the comparison of liquid volume fraction at various locations from the inlet of the channel. vof-0.1 indicates liquid volume fraction values taken at a distance of 10 mm from the inlet. From the figure, it can be seen that the liquid volume fraction changes sharply from 0 to 1 across the interface which is at 0.031 m. This indicates that the interface is smooth without any waves. Figure 4.2 shows the smooth stratified, horizontal flow pattern obtained in the simulation. Figures 4.1 and 4.2 are taken from the simulation in which the coarse mesh used.

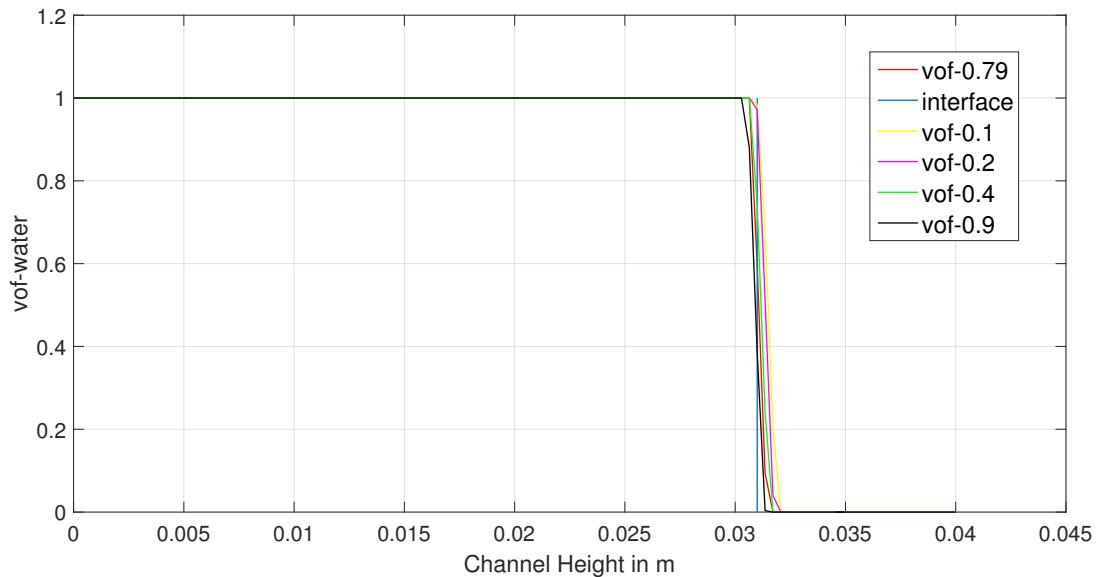


**Figure 4.1:** Liquid volume fraction comparison at various locations across the channel.

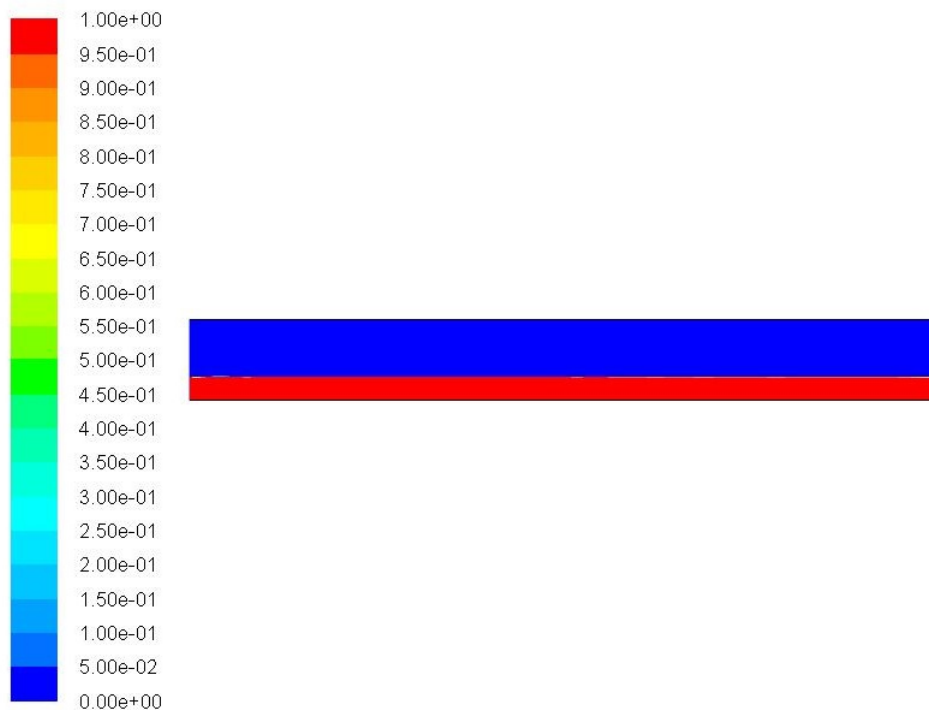


**Figure 4.2:** Liquid volume fraction in the channel

The comparison of the temperature profiles of all the cases simulated against experimental data is presented in Figure 4.3. The temperature profile is taken at the probe location i.e. 790 mm from the inlet of the channel. The temperature profile is taken only till 40 mm of the channel height, because the upper part of the channel is filled with saturated steam and is not relevant for the comparison. The temperature profiles in all the cases have similar profile as in experiment as shown in Figure 4.3, but the thermal layer in the liquid is very thin compared to the experimental data. The temperature profile obtained for both coarse mesh and fine mesh (i.e. case-1 and case-2) are almost similar. This indicates that the calculations were mesh independent.

Case-1 and case-3 are solved using the coarse mesh but with different condensation models. It can be inferred from Figure 4.3 that the temperature profile obtained in two cases are almost similar. A closer look at the temperature profile in Figure 4.3 near the interface will reveal that case-3 i.e. simulation using Shen et al. model has high temperature at the interface and is close to the experiment. This can also be seen in Figure 4.4. Even though the temperature profile looks similar to the experiment in both cases, none of them predicted a similar thermal layer in liquid. The probable explanation for the the failure of the model is the calculation of turbulence quantities in the liquid. The heat transfer coefficient is calculated based on the turbulence characteristics of the liquid in both models and the VOF method have limitations resolving the momentum equation at the interface, if the relative velocity between two phases is high. One more probable explanation might be the usage of turbulence damping to get a smooth stratified flow. Turbulence damping damps all the turbulence quantities near the interface and this affects the calculation of HTC.

Calculation of the HTC isn't the only limiting factor but also the spreading of the thermal boundary layer. The calculated heat transfer might be sufficient to heat up the first cell but the liquid is not mixing sufficiently.

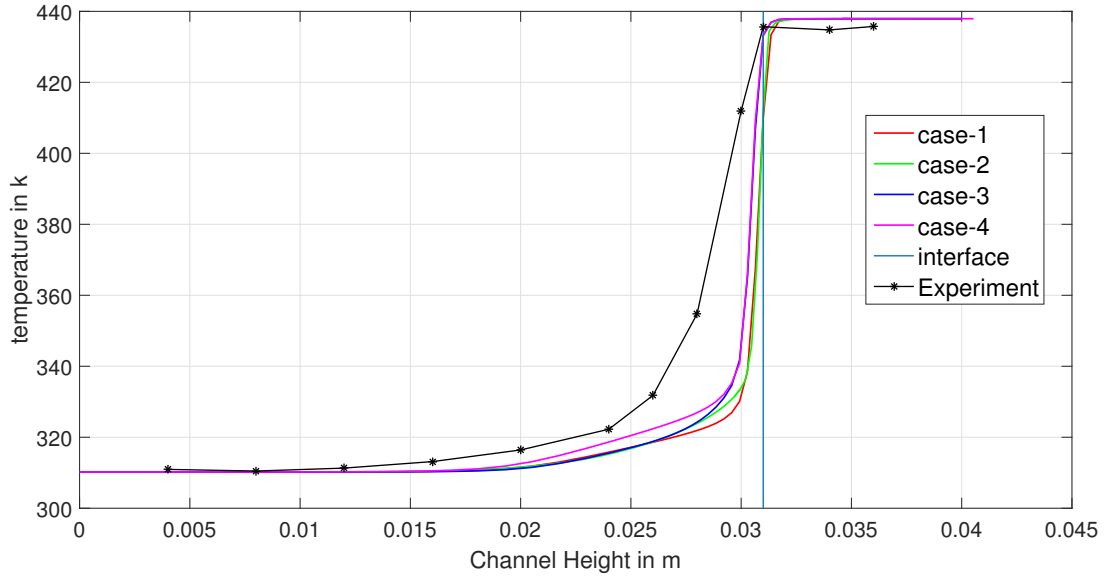


**Figure 4.3:** Comparison of the temperature profiles against LAOKOON experimental data.

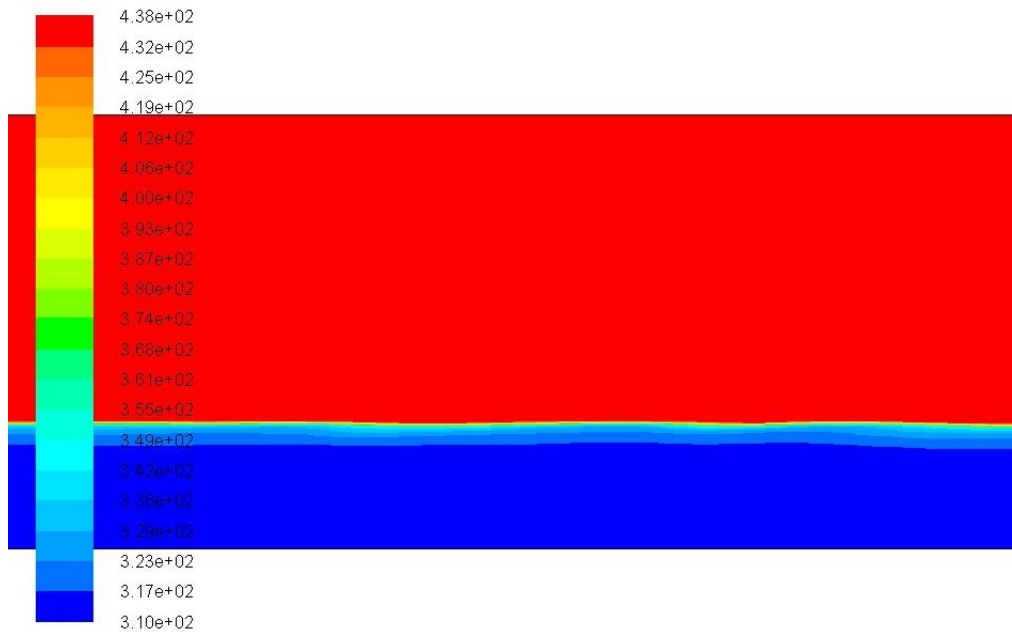


**Figure 4.4:** Closer view of temperature profile in case-3.

Figure 4.5 shows a direct comparison of the heat transfer coefficient calculated with two models. The difference between the calculated HTC is obvious because the

Hughes and Duffey model uses Kolmogorov scales which will result in shorter surface renewal time, whereas the shen et al. model uses larger eddies which will result in larger surface renewal time. The HTC calculated with the Hughes and Duffey is high compared to the Shen et al. model, this should result in more heat and mass transfer with the Hughes model according to theory. But, this is not the case with simulation results obtained, the temperature profile obtained with the shen et al. model is slightly closer to the experiment compared to the Hughes model. From this, one can infer that calculation of HTC is not the only limiting factor. The effect of turbulence damping can also be seen in Figure 4.5. HTC calculated using the Hughes and Duffey model has a sharp increase in the liquid side near the interface. The simulation with modified energy source has better temperature profile compared to other cases. This might be because of accurate calculation of the energy source term (i.e., heat transfer) during phase change.

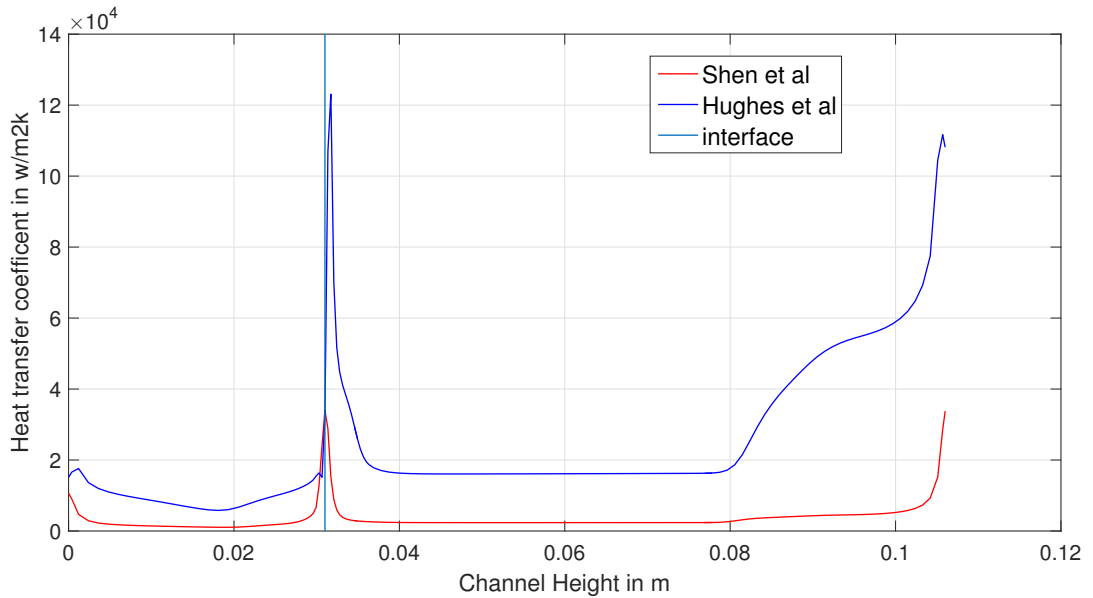


**Figure 4.5:** Comparison between the HTC calculated at probe location with both condensation models

A fully converged solution is not achieved in any of the simulations. There is always some mass imbalance in the liquid phase. This can also be seen in Figure 4.6 in which liquid mass balance ( $m_{fin} - m_{fout}$ ) and mass condensed in the channel are plotted over time. The mass is perfectly balanced in the gas phase. This might also be one of the reason why the simulation results are not closer to the experiment. The overall mass condensed in the channel is partially converged, as shown in Figure 4.6. The initial ramp in the mass condensed value is because of the implementation of the ramp function in the simulation.

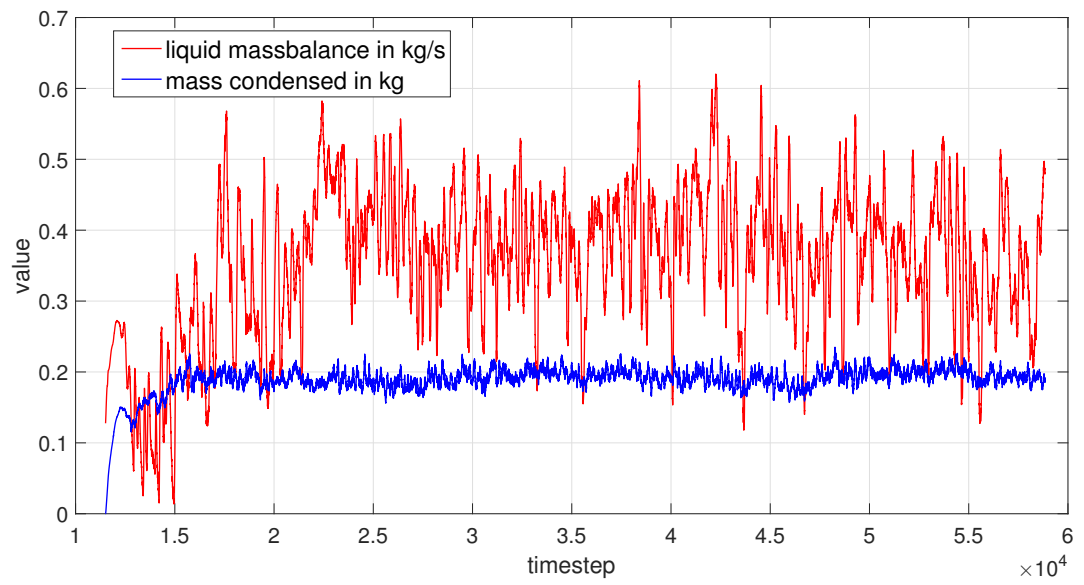


Figure 4.6: Convergence plot for case-1



# 5

## Conclusion

Simulations of the LAOKOON experimental facility have been performed to study DCC phenomenon. Two condensation models based on surface renewal theory are used to calculate the phase change in the channel. The focus of the work is set only on the implementation and studying the performance of the condensation models. Other aspects, like the impact of turbulence model and calculation of the interfacial area density are not considered in the study. The temperature profiles obtained in the simulations corresponds well to the experimental profile, but the thermal layer obtained in the simulations is thinner than in the experiment. The choice of using turbulence damping is necessary to achieve a smooth surface without waves. However, in a phenomenon like condensation induced water hammer, one expect waves to form on the surface. To conclude, the performance of these models should be studied without using turbulence damping before they are used to simulate CIWH phenomenon.

### 5.1 Future work

Further benchmarking needs to be done to know the performance of condensation models. It would be interesting to see how both condensation models will behave without turbulence damping. More validation of the condensation models should be done with the experiments where waves are expected on the surface. It would also be interesting to study the simulations where the surface renewal time is varied in the calculations based on key parameters, like the liquid turbulence. Since condensation models are based on liquid turbulence properties, it would be interesting to study the effect of various turbulence models.



# Bibliography

- [1] “Steam Condensation Induced Water hammer”, Jan ’98 HPAC Article by Wayne Kirsner, P.E.
- [2] W. Streicher, “Minimising the risk of water hammer and other problems at the beginning of stagnation of solar thermal plants- a theoretical approach”, *Solar Energy*, 69, 187-196 (2000).
- [3] R. Scardovelli, S. Zaleski, “Direct numerical simulation of free-surface and interfacial flow”, *Annual Review of Fluid Mechanics*, 31, 567-603 (1999).
- [4] P. Smereka, J. A. Sethian, “Level set methods for fluid interfaces”, *Annual Review of Fluid Mechanics* 35, 341-372 (2003).
- [5] O. Unverdi, G. Tryggvason, “A front-tracking method for viscous, incompressible, multi-fluid flows”, *Journal of Computational Physics*, 100, 25-37 (1992).
- [6] Sabin-Cristian Ceuca, “Computational Simulations of Direct contact condensation as the driving force for Water hammer”, Ph.D, Technische Universität München 2015.
- [7] E.D. Hughes and R.B. Duffey. “Direct Contact Condensation and Momentum Transfer in Turbulent Separated Flows”. *International Journal Multiphase Flow*, 17:599-619, 1991.
- [8] R. Higbie. “The Rate of Absorption of a Pure Gas into a Still Liquid during a Short Time of Exposure”. *Transactions of the American Institute of Chemical Engineers*, 31:365-389, 1935.
- [9] L. Shen, G.S. Triantafyllou, and D.K.P. Yue. “Turbulent Diffusion near a Free Surface”. *Journal of Fluid Mechanics*, 407:145-166, 2000.
- [10] L.T. Fan, B.C. Shen and S.T. Chou “The Surface-renewal theory of interphase transport- a stochastic phenomenon” *Chem. Eng. Sci.*, 48, 3971-3982 (1993).
- [11] L. Štrubelj, Gy. Ézsöl, and I. Tiselj. “Direct Contact Condensation Induced Transition from Stratified to Slug Flow”. *Nuclear Engineering and Design*, 240:266–274, 2010.
- [12] Coste, P., et al., “Modeling Turbulence and Friction around a Large Interface in a Three- Dimension Two- Velocity Eulerian Code”, Proc. of NURETH 12, Pittsburgh, USA (2007).
- [13] P. Coste, J. Pouvreau, J. Laviéville, M. Boucker, “A Two-phase cfd approach to the PTS problem evaluated on COSI experiment”, *Proceedings of the 16th International Conference on Nuclear Engineering ICONE16*, May 11-15, 2008, Orlando, Florida, USA (2008).
- [14] Strubelj, L., Tiselj, I. (2008). “Numerical modelling of direct contact condensation in transition from stratified to slug flow”. *Computational Fluid Dynamics (CFD) in Nuclear Reactor Safety (NRS) - Proceedings of the workshop on Ex-*

- periments and CFD Code Application to Nuclear Reactor Safety (XCFD4NRS)*, (p. 1027). Nuclear Energy Agency of the OECD (NEA)
- [15] Rita Sziártó, “Condensation of steam in horizontal pipes - model development and validation”, Ph.D, ETH Zurich 2015.
- [16] W. H. Lee. “A Pressure Iteration Scheme for Two-Phase Flow Modeling”. In: *Multiphase Transport: Fundamentals, Reactor Safety, Applications*, pages 407–432, 1980.
- [17] Arnaldo Badillo. “Quantitative phase-field modeling for boiling phenomena”. *Physical Review E*, 86:041603, Oct 2012.
- [18] John R. Thome. “Engineering Data Book III”. Wolverine Tube, Inc Online, 2010.
- [19] Rouhani, S. Z., and Sohal, M. S., 1983, “Two-Phase Flow Patterns: A Review of Research Results,” *Prog. Nucl. Energy*, 11 (3), pp. 219–259.
- [20] C.W. Hirt and B.D. Nichols. “Volume of Fluid (VOF) Method for the Dynamics of Free Boundaries”. *Journal of Computational Physics*, 39:207-225, 1981.
- [21] Jeon, S.S., Kim, S.J. and Park, G.C., 2009. “CFD simulation of condensing vapor bubble using VOF model”, *World Acad. Sci. Eng. Technol.*, 3, 12–27 .
- [22] Danckwerts, P.V., 1951 Significance of liquid-film coefficient in gas absorption; 12. *Engng Chem.*43, 1460-1467.
- [23] Duffey, R.B., and Hughes, E.D. (1995). *Gas mass transfer for stratified flows (BNL–61801)*. United States
- [24] Kitaigorodskii, S.A. and Donelan, M.A. 1984, “Wind-wave effects on gas transfer,” in *Gas Transfer at Water Surfaces*, edited by W. Brutsaert and G. H. Jirka, pp. 147-170, D. ReidelPublishing Co., Norwell, Mass.
- [25] Banerjee, S. 1978 “A surface renewal model for interfacial heat and mass transfer in transient two-phase flow”. *Int. J. Multiphase Flow* 4, 571-573.
- [26] M. Goldbrunner, J. Karl, and D. Hein. “Experimental Investigation of Heat Transfer Phenomena During Direct Contact Condensation in the Presence of Noncondensable gas by means of Linear Raman Spectroscopy”. In 10th Int. Symp. on Laser Techniques Applied to Fluid Mechanics, Lisbon, July 2000.
- [27] D. Lucas. “Review of the existing data basis for the validation of models for PTS”. Technical Report NURESIM-SP2-TY; D2.1.2, FZR, 2005.
- [28] ANSYS, Inc. ANSYS FLUENT 16.1: User’s Guide.
- [29] Weisman J.(1983). “Two-phase flow patterns”. In *Handbook of fluids in motion*,pp.409-25 (eds.N.P.Cheremisinoff and R. Gupts).Ann Arbor Science.
- [30] S. C. Ceuca and Macián-Juan R. “CFD Simulation of Direct contact Condensation with ANSYS CFX using Locally defined Heat Transfer Coefficient”. *Proceedings of the 20th International Conference on Nuclear Engineering collocated with the ASME 2012 Power Conference*, 2012.
- [31] S.Hardt and F.Wondra. “Evaporation model for interfacial flows based on a continuum field representation of the source terms”. *Journal of Computational Physics*, 227:5871– 5895, 2008
- [32] U.S. NRC. *RELAP5/mod3.3 Code Manual Vol. IV.: Models and Correlations*, 2001. NUREG/CR-5535/Rev-1.
- [33] U. S. NRC. *TRACE V5.0p2: TheoryManual*, 2010.

# A

## Appendix 1

### A.1 User Defined Functions used

In total, four UDFs are used in the calculations.

#### UDF for calculating Interfacial Area density

*DEFINE\_ADJUST* UDF is used for the calculation of Interfacial area density. IAD is calculated and stored in user defined memory to call into other UDF's.

```
1
2 #include "udf.h"
3 DEFINE_ADJUST(gradient , domain)
4
5 {
6
7 #if !RP_HOST
8
9 Thread *t;
10
11 Thread **pt;
12
13 cell_t c;
14
15 int phase_domain_index = 0;
16 /* Check the phase every time whether it is primary or secondary */
17 Domain *pDomain = DOMAIN_SUB_DOMAIN(domain,phase_domain_index);
18
19 {
20
21     Alloc_Storage_Vars (pDomain ,SV_VOF_RG,SV_VOF_G,SV_NULL) ;
22
23     Scalar_Reconstruction (pDomain , SV_VOF, -1,SV_VOF_RG,NULL) ;
24
25     Scalar_Derivatives (pDomain ,SV_VOF, -1,SV_VOF_G,SV_VOF_RG,
26         Vof_Deriv_Accumulate) ;
27 }
28
29 mp_thread_loop_c (t , domain , pt)
30
31 if (FLUID_THREAD_P(t))
32
33 {
```

```

34 Thread *ppt = pt[phase_domain_index];
35
36 begin_c_loop (c,t)
37 {
38
39     {
40
41         C_UDMI(c,t,0) = sqrt((C_VOF_G(c,ppt)[0]*C_VOF_G(c,ppt)[0])+(
42         C_VOF_G(c,ppt)[1]*C_VOF_G(c,ppt)[1]));
43     }
44
45 end_c_loop (c,t)
46
47 }
48
49 Free_Storage_Vars(pDomain,SV_VOF_RG,SV_VOF_G,SV_NULL);
50 #endif
51 }

```

## UDF for mass source term

Two UDFs are used for mass source term. The liquid mass and gas mass source terms are passed directly to phase specific threads in Fluent. All the thermo-physical properties are hardcoded. They can also be called using various macros in Fluent. Mass transfer is calculated in the energy source UDF and is passed using UDM.

### Liquid mass source term

```

1 #include "udf.h"
2 DEFINE_SOURCE(liq_src,c,liq_th,dS,eqn) /*liquid source udf*/
3 {
4     real m_l;
5     real h_lt = 2064920.0;
6     Thread *t, *gas_th;
7     t = THREAD_SUPER_THREAD(liq_th);
8     gas_th = THREAD_SUB_THREAD(t,1);
9     m_l = 0.0;
10    m_l = C_UDMI(c,t,8)/h_lt;
11    dS[eqn] = 0.0;
12    C_UDMI(c,t,9) = m_l;
13    return (m_l);
14 }

```

### Gas mass source term

```

1 #include "udf.h"
2 DEFINE_SOURCE(gas_src,c,gas_th,dS,eqn) /*gas source udf*/
3 {
4     real m_v;
5     Thread *t, *liq_th;
6     real h_lt = 2064920.0;
7     t = THREAD_SUPER_THREAD(gas_th);
8     liq_th = THREAD_SUB_THREAD(t,0);

```

```

9   m_v = 0.0;
10  m_v = -C_UDMI(c,t,8)/h_lt;
11  dS[eqn] = 0.0;
12  C_UDMI(c,t,10) = m_v;
13  return (m_v);
14 }

```

## UDF for energy source term

Energy source term is passed to the mixture level thread. The heat transfer is stored in UDM and passed to mass source UDFs using UDM to calculate mass transfer.

```

1 #include "udf.h"
2 DEFINE_SOURCE(enrg_src_in,c,t,dS,eqn) /*energy source udf*/
3 {
4
5   Thread *liq_th, *gas_th;
6   liq_th = THREAD_SUB_THREAD(t,0);
7   gas_th = THREAD_SUB_THREAD(t,1);
8   real m_s;
9   m_s = 0.0;
10  real T_l = 0.0;
11  T_l = C_T(c,liq_th); /* local liquid temperature */
12  real Tsat = 437.93;
13  real h_lt = 2064920.0;
14  real rho_l = 996.77; /* liquid density */
15  real theCond_l = 0.6109; /* liquid thermal conductivity */
16  real kinVisc_l = 0.00084/rho_l; /* liquid kinematic viscosity */
17  real disspl_l = 0.09*C_K(c,liq_th)*C_O(c,liq_th); /* dissipation */
18  real speheat_l = 4179.0; /* liquid specific heat capacity */
19  real vof_cutoff = 0.0001;
20  real htc;
21  htc = 0.0;
22  real ai = 0.0;
23  real Qtransfer = 0.0;
24  if (C_VOF(c,liq_th) > vof_cutoff && C_VOF(c,liq_th) < (1-vof_cutoff))
25  {
26    htc = (2/sqrt(3.14))*(sqrt(rho_l*speheat_l*theCond_l))*pow((
27      disspl_l/kinVisc_l),0.25);
28
29    ai = C_UDMI(c,t,0);
30    if (ai > 1 && (Tsat-T_l) > 0.00001)
31    {
32      Qtransfer= (htc*ai*(Tsat-T_l));
33      C_UDMI(c,t,11) = htc;
34      C_UDMI(c,t,12) = (Tsat-T_l);
35    }
36  }
37  else
38  {
39    Qtransfer = 0;
40  }
41  }
42  else
43  {
44    Qtransfer = 0;

```

```
43 }
44 int cur_time ;
45 int old_time ;
46 real phy_time ;
47 cur_time = N_TIME;
48 phy_time = CURRENT_TIME;
49 old_time = C_UDMI(c,t,7) ;
50 C_UDMI(c,t,1) = Qtransfer;
51
52 if ( cur_time != old_time)
53 {
54     C_UDMI(c,t,7) = cur_time;
55     C_UDMI(c,t,6) = C_UDMI(c,t,5); /* dQ at t-5*/
56     C_UDMI(c,t,5) = C_UDMI(c,t,4); /* dQ at t-4*/
57     C_UDMI(c,t,4) = C_UDMI(c,t,3); /*dQ at t-3*/
58     C_UDMI(c,t,3) = C_UDMI(c,t,2); /* dQ at t-2*/
59     C_UDMI(c,t,2) = C_UDMI(c,t,1); /* dQ at t-1*/
60 }
61
62
63 real rampStart = 1.845; /*Ramp function*/
64 real rampVal = 2.00;
65
66 real ft = 0.0;
67
68 if (phy_time < (rampVal+rampStart) && (phy_time > rampStart))
69 {
70     ft=(phy_time-rampStart)/2;
71 }
72 else if ( phy_time < rampStart )
73 {
74     ft = 0;
75 }
76 else
77 {
78     ft = 1;
79 }
80
81 m_s = ft*( Qtransfer+C_UDMI(c,t,2)+C_UDMI(c,t,3)+C_UDMI(c,t,4)+C_UDMI(c
82 ,t,5)+C_UDMI(c,t,6) )/6;
83 C_UDMI(c,t,8) = m_s;
84 dS[eqn] = 0.0;
85
86 return (m_s);
87 }
```

## A.2 Smearing Function

As discussed in the previous chapters, introducing mass transfer only at the interface will result in convergence problems. Hardt and Wondra[31] suggested an approach to smear the mass and heat transfer to neighbouring cells by solving a diffusion equation for mass transfer. The diffusion equation was solved in the domain with

the Neumann boundary condition, which states that the flux is zero at the domain ( $\Omega$ ) boundaries. The diffusion equation which is solved is shown below

$$\nabla\varphi = \frac{1}{D}(\varphi - \varphi_0),$$

where  $\varphi_0 = \dot{m}$  (original mass transfer),  $\varphi$  is the diffused mass transfer and  $D$  is the diffusion coefficient.

The length of smearing is controlled by the diffusion coefficient  $D$ . The mass transfer ( $S_m$ ) and energy source term ( $S_e$ ) are calculated as below,

$$\begin{aligned} S_m &= N_v\alpha_v\varphi - N_l\alpha_l\varphi, \\ N_v &= \frac{\int_{\Omega} \varphi d\Omega}{\int_{\Omega} \alpha_v\varphi d\Omega}, \\ N_l &= \frac{\int_{\Omega} \varphi d\Omega}{\int_{\Omega} \alpha_l\varphi d\Omega}, \end{aligned}$$

where  $N_l$  and  $N_v$  are normalization factors that ensure the mass appeared in the liquid phase is same as mass disappeared from the gas phase.

The energy source term contains two parts, one due to phase change and a correction term that accounts for the decreased enthalpy flux due to the decreased mass flux in the phase change region.

$$\begin{aligned} S_e &= S_e^p + S_e^c, \\ S_e^p &= -h_{lv}N_l^0\alpha_l\varphi_0, \\ N_l^0 &= \frac{\int_{\Omega} \varphi_0 d\Omega}{\int_{\Omega} \alpha_l\varphi d\Omega}, \\ S_e^c &= (N_v\alpha_vC_{pl} - N_l\alpha_lC_{pl})T\varphi. \end{aligned}$$

This method is also tried to solve convergence issues, but this did not solve the convergence issues completely. The simulation ran without any stability and convergence issues if the time step size is small, but this resulted in increase of computational time and small pressure fluctuations.